Research Article | Vol. 25, No. 8 | 17 Apr 2017 | OPTICS EXPRESS A311

Optics EXPRESS

Modeling and designing multilayer 2D perovskite / silicon bifacial tandem photovoltaics for high efficiencies and long-term stability

HAEJUN CHUNG,[1] XINGSHU SUN,[1] ADITYA D. MOHITE,[2] RAHUL SINGH,[3] LOKENDRA KUMAR,[4] MUHAMMAD A. ALAM,[1] AND PETER BERMEL[1,*]

[1]*Birck Nanotechnology Center, 1205 W. State St, West Lafayette, Indiana, USA*
[2]*Los Alamos National Laboratory, Los Alamos, NM 87545, USA*
[3]*Centre for Ionics University of Malaya, Department of Physics, Faculty of Science, University of Malaya, 50603 Kuala Lumpur, Malaysia*
[4]*Department of Physics, Science Faculty University of Allahabad, Allahabad-211 002 India*
[*]*pbermel@purdue.edu*

Abstract: A key challenge in photovoltaics today is to develop cell technologies with both higher efficiencies and lower fabrication costs than incumbent crystalline silicon (c-Si) single-junction cells. While tandem cells have higher efficiencies than c-Si alone, it is generally challenging to find a low-cost, high-performance material to pair with c-Si. However, the recent emergence of 22% efficient perovskite photovoltaics has created a tremendous opportunity for high-performance, low-cost perovskite / crystalline silicon tandem photovoltaic cells. Nonetheless, two key challenges remain. First, integrating perovskites into tandem structures has not yet been demonstrated to yield performance exceeding commercially available crystalline silicon modules. Second, the stability of perovskites is inconsistent with the needs of most end-users, who install photovoltaic modules to produce power for 25 years or more. Making these cells viable thus requires innovation in materials processing, device design, fabrication, and yield. We will address these two gaps in the photovoltaic literature by investigating new types of 2D perovskite materials with *n*-butylammonium spacer layers, and integrating these materials into bifacial tandem solar cells providing at least 30% normalized power production. We find that an optimized 2D perovskite ($(BA)_2(MA)_3(Sn_{0.6}Pb_{0.4})_4I_{13}$)/silicon bifacial tandem cell, given a globally average albedo of 30%, yields a normalized power production of 30.31%, which should be stable for extended time periods without further change in materials or encapsulation.

OCIS codes: (350.4238) Nanophotonics and photonic crystals; (350.6050) Solar energy.

References and links

1. H.-S. Kim, C.-R. Lee, J.-H. Im, K.-B. Lee, T. Moehl, A. Marchioro, S.-J. Moon, R. Humphry-Baker, J.-H. Yum, J. E. Moser, M. Grätzel, and N.-G. Park, "Lead iodide perovskite sensitized all-solid-state submicron thin film mesoscopic solar cell with efficiency exceeding 9%," Sci. Rep. **2**, 591 (2012).
2. M. M. Lee, J. Teuscher, T. Miyasaka, T. N. Murakami, and H. J. Snaith, "Efficient hybrid solar cells based on meso-superstructured organometal halide perovskites," Science **338**, 643–647 (2012).
3. Y. Zhou and K. Zhu, "Perovskite solar cells shine in the valley of the sun," ACS Energy Lett. **1**, 64–67 (2016).
4. J. P. Mailoa, C. D. Bailie, E. C. Johlin, E. T. Hoke, A. J. Akey, W. H. Nguyen, M. D. McGehee, and T. Buonassisi, "A 2-terminal perovskite/silicon multijunction solar cell enabled by a silicon tunnel junction," Appl. Phys. Lett. **106**, 121105 (2015).
5. J. Werner, C.-H. Weng, A. Walter, L. Fesquet, J. P. Seif, S. De Wolf, B. Niesen, and C. Ballif, "Efficient monolithic perovskite/silicon tandem solar cell with cell area> 1 cm2," J. Phys. Chem. Lett. **7**, 161–166 (2015).
6. H. Zhou, Q. Chen, G. Li, S. Luo, T.-b. Song, H.-S. Duan, Z. Hong, J. You, Y. Liu, and Y. Yang, "Interface engineering of highly efficient perovskite solar cells," Science **345**, 542–546 (2014).
7. S. J. Lee, S. S. Shin, Y. C. Kim, D. Kim, T. K. Ahn, J. H. Noh, J. Seo, and S. I. Seok, "Fabrication of efficient formamidinium tin iodide perovskite solar cells through snf2–pyrazine complex," J. American Chem. Soc. **138**, 3974–3977 (2016).

#284405 https://doi.org/10.1364/OE.25.00A311
Journal © 2017 Received 17 Jan 2017; revised 22 Feb 2017; accepted 24 Feb 2017; published 14 Mar 2017

Optics EXPRESS

8. W. Nie, H. Tsai, R. Asadpour, J.-C. Blancon, A. J. Neukirch, G. Gupta, J. J. Crochet, M. Chhowalla, S. Tretiak, M. A. Alam, H.-L. Wang, and A. D. Mohite, "High-efficiency solution-processed perovskite solar cells with millimeter-scale grains," Science **347**, 522–525 (2015).
9. W. Nie, J.-C. Blancon, A. J. Neukirch, K. Appavoo, H. Tsai, M. Chhowalla, M. A. Alam, M. Y. Sfeir, C. Katan, J. Even, S. Tretiak, J. J. Crochet, G. Gupta, and A. D. Mohite, "Light-activated photocurrent degradation and self-healing in perovskite solar cells," Nat. Commun. **7**, 11574 (2016).
10. H. Tsai, W. Nie, J.-C. Blancon, C. C. Stoumpos, R. Asadpour, B. Harutyunyan, A. J. Neukirch, R. Verduzco, J. J. Crochet, S. Tretiak, L. Pedesseau, J. Even, M. A. Alam, G. Gupta, J. Lou, P. M. Ajayan, M. J. Bedzyk, M. G. Kanatzidis, and A. D. Mohite, "High-efficiency two-dimensional ruddlesden–popper perovskite solar cells," Nature **536**, 312–316 (2016).
11. K. A. Bush, C. D. Bailie, Y. Chen, A. R. Bowring, W. Wang, W. Ma, T. Leijtens, F. Moghadam, and M. D. McGehee, "Thermal and environmental stability of semi-transparent perovskite solar cells for tandems enabled by a solution-processed nanoparticle buffer layer and sputtered ito electrode," Adv. Mat. **28**, 3937–3943 (2016).
12. S. A. Gevorgyan, M. V. Madsen, H. F. Dam, M. Jørgensen, C. J. Fell, K. F. Anderson, B. C. Duck, A. Mescheloff, E. A. Katz, A. Elschner, R. Roeschf, H. Hoppef, M. Hermenaug, M. Riedeg, and F. C. Krebsa, "Interlaboratory outdoor stability studies of flexible roll-to-roll coated organic photovoltaic modules: Stability over 10,000 h," Sol. Energy Mat. Sol. Cells **116**, 187–196 (2013).
13. C. L. Uhrich, G. Schwartz, B. Maennig, W. M. Gnehr, S. Sonntag, O. Erfurth, E. Wollrab, K. Walzer, J. Foerster, A. Weiss, O. Tsaryova, K. Leo, M. K. Riede, and M. Pfeiffer, "Efficient and long-term stable organic vacuum deposited tandem solar cells," in *SPIE Photonics Europe* (International Society for Optics and Photonics, 2010), paper 77220G.
14. I. Almansouri, A. Ho-Baillie, and M. A. Green, "Ultimate efficiency limit of single-junction perovskite and dual-junction perovskite/silicon two-terminal devices," Jpn. J. Appl. Phys. **54**, 08KD04 (2015).
15. R. Asadpour, R. V. Chavali, M. R. Khan, and M. A. Alam, "Bifacial si heterojunction-perovskite organic-inorganic tandem to produce highly efficient (ηt* 33%) solar cell," Appl. Phys. Lett. **106**, 243902 (2015).
16. S. Albrecht, M. Saliba, J. P. C. Baena, F. Lang, L. Kegelmann, M. Mews, L. Steier, A. Abate, J. Rappich, L. Korte, R. Schlatmann, M. K. Nazeeruddin, A. Hagfeldt, M. GrÃd'tzeld, and B. Recha, "Monolithic perovskite/silicon-heterojunction tandem solar cells processed at low temperature," Energy Environ. Sci. **9**, 81–88 (2016).
17. P. Löper, S.-J. Moon, S. M. De Nicolas, B. Niesen, M. Ledinsky, S. Nicolay, J. Bailat, J.-H. Yum, S. De Wolf, and C. Ballif, "Organic–inorganic halide perovskite/crystalline silicon four-terminal tandem solar cells," Phys. Chem. Chem. Phys.**17**, 1619–1629 (2015).
18. C. D. Bailie, M. G. Christoforo, J. P. Mailoa, A. R. Bowring, E. L. Unger, W. H. Nguyen, J. Burschka, N. Pellet, J. Z. Lee, M. Grätzel, R. Noufi, T. Buonassisi, A. Salleoa, and M. D.McGehee, "Semi-transparent perovskite solar cells for tandems with silicon and cigs," Energy Environ. Sci. **8**, 956–963 (2015).
19. J. Werner, L. Barraud, A. Walter, M. BrÃd'uninger, F. Sahli, D. Sacchetto, N. TÃl'treault, B. Paviet-Salomon, S.-J. Moon, C. AllebeÌĄ, M. Despeisse, S. Nicolay, S. De Wolf, B. Niesen, and C. Ballif, "Efficient near-infrared-transparent perovskite solar cells enabling direct comparison of 4-terminal and monolithic perovskite/silicon tandem cells," ACS Energy Lett. **1**, 474–480 (2016).
20. H. Uzu, M. Ichikawa, M. Hino, K. Nakano, T. Meguro, J. L. Hernández, H.-S. Kim, N.-G. Park, and K. Yamamoto, "High efficiency solar cells combining a perovskite and a silicon heterojunction solar cells via an optical splitting system," Appl. Phys. Lett. **106**, 013506 (2015).
21. H. Chung, X. Sun, and P. Bermel, "Optical approaches to improving perovskite/si tandem cells," MRS Adv. **1**, 901–910 (2016).
22. M. R. Khan and M. A. Alam, "Thermodynamic limit of bifacial double-junction tandem solar cells," Appl. Phys. Lett. **107**, 223502 (2015).
23. B. A. Wielicki, T. Wong, N. Loeb, P. Minnis, K. Priestley, and R. Kandel, "Changes in earth's albedo measured by satellite," Science **308**, 825 (2005).
24. B. W. Schneider, N. N. Lal, S. Baker-Finch, and T. P. White, "Pyramidal surface textures for light trapping and antireflection in perovskite-on-silicon tandem solar cells," Opt. Express **22**, A1422–A1430 (2014).
25. Y. Z. Dai Shi and W. Shen, "Perovskite/c-si tandem solar cell with inverted nanopyramids: realizing high efficiency by controllable light trapping," Sci. Rep. **5**, 16504 (2015).
26. Y. Zhang and Y. Xuan, "Comprehensive design of omnidirectional high-performance perovskite solar cells," Sci. Rep. **6**, 29705 (2016).
27. B. Cai, Y. Peng, Y.-B. Cheng, and M. Gu, "4-fold photocurrent enhancement in ultrathin nanoplasmonic perovskite solar cells," Opt. Express **23**, A1700–A1706 (2015).
28. M. Filipič, P. Löper, B. Niesen, S. De Wolf, J. Krč, C. Ballif, and M. Topič, "Ch 3 nh 3 pbi 3 perovskite/silicon tandem solar cells: characterization based optical simulations," Opt. Express **23**, A263–A278 (2015).
29. Y. Jiang, M. A. Green, R. Sheng, and A. Ho-Baillie, "Room temperature optical properties of organic–inorganic lead halide perovskites," Sol. Energy Mat. Sol. Cells **137**, 253–257 (2015).
30. A. J. Moulé and K. Meerholz, "Interference method for the determination of the complex refractive index of thin polymer layers," Appl. Phys. Lett. **91**, 061901 (2007).
31. A. Tavlove and S. C. Hagness, *Computational Electrodynamics: The Finite-difference Time-domain Method* (Artech House, 1995).

Optics EXPRESS

32. G. Jellison Jr. and F. Modine, "Parameterization of the optical functions of amorphous materials in the interband region," Appl. Phys. Lett. **69**, 371–373 (1996).
33. H. Chung, S.-G. Ha, J. Choi, and K.-Y. Jung, "Accurate fdtd modelling for dispersive media using rational function and particle swarm optimisation," Int. J. Electronics **102**, 1218–1228 (2015).
34. H. Chung, C. Zhou, X. Tee, K. Jung, and P. Bermel, "Hybrid dielectric light trapping designs for thin-film cdznte/si tandem cells," Opt. Express **24**, A1008–A1020 (2016).
35. J. Cho, S.-G. Ha, Y. B. Park, H. Kim, and K.-Y. Jung, "On the numerical stability of finite-difference time-domain for wave propagation in dispersive media using quadratic complex rational function," Electromagnetics **34**, 625–632 (2014).
36. S. J. Orfanidis, *Electromagnetic Waves and Antennas* (Rutgers University, 2002).
37. H. Chung, K. Jung, X. Tee, and P. Bermel, "Time domain simulation of tandem silicon solar cells with optimal textured light trapping enabled by the quadratic complex rational function," Opt. Express **22**, A818–A832 (2014).
38. H. Tan, R. Santbergen, A. H. Smets, and M. Zeman, "Plasmonic light trapping in thin-film silicon solar cells with improved self-assembled silver nanoparticles," Nano Lett. **12**, 4070–4076 (2012).
39. B. Chen, Y. Bai, Z. Yu, T. Li, X. Zheng, Q. Dong, L. Shen, M. Boccard, A. Gruverman, and Z. Holman "Efficient semitransparent perovskite solar cells for 23.0%-efficiency perovskite/silicon four-terminal tandem cells," Adv. Energy Mat. **6**, 1601128 (2016).
40. B. Zhao, M. Abdi-Jalebi, M. Tabachnyk, H. Glass, V. S. Kamboj, W. A. Nie, J. Pearson, Y. Puttisong, K. C. Gödel, H. E. Beere, D. A. Ritchie, A. D. Mohite, S. E. Dutton, R. H. Friend, and A. Sadhanala, "High open-circuit voltages in tin-rich low-bandgap perovskite-based planar heterojunction photovoltaics," Adv. Mat. **29**(2), 1604744 (2016).
41. X. Sun, R. Asadpour, W. Nie, A. D. Mohite, and M. A. Alam, "A physics-based analytical model for perovskite solar cells," IEEE J. Photovolt. **5**, 1389–1394 (2015).
42. M. Brennan, A. Abramase, R. W. Andrews, and J. M. Pearce, "Effects of spectral albedo on solar photovoltaic devices," Sol. Energy Mat. Sol. Cells **124**, 111–116 (2014).
43. M. Taguchi, A. Yano, S. Tohoda, K. Matsuyama, Y. Nakamura, T. Nishiwaki, K. Fujita, and E. Maruyama, "24.7% record efficiency hit solar cell on thin silicon wafer," IEEE J. Photovolt. **4**, 96–99 (2014).
44. M. A. Green, K. Emery, Y. Hishikawa, W. Warta, and E. D. Dunlop, "Solar cell efficiency tables (version 47)," Progress Photovolt.: Res. Appl. **24**, 3–11 (2016).
45. D. Grant, K. Catchpole, K. Weber, and T. White, "Design guidelines for perovskite/silicon 2-terminal tandem solar cells: an optical study," Opt. Express **24**, A1454–A1470 (2016).
46. R. V. K. Chavali, S. Khatavkar, C. Kannan, V. Kumar, P. R. Nair, J. L. Gray, and M. A. Alam, "Multiprobe characterization of inversion charge for self-consistent parameterization of hit cells," IEEE J. Photovolt. **5**, 725–735 (2015).

1. Introduction

Metal-halide perovskites have gained a great deal of attention for their extraordinarily rapid increase in single junction world-record efficiencies, rising from below 1% to 22% today [1–3]. Similarly, world-record cell efficiencies of perovskite/silicon tandem cells have risen from 13% [4] to over 21% [5] within a little over one year. Furthermore, perovskites are solution-processable materials that appear resilient in the presence of defects [1, 2]; thus, they have a potential to serve as ultra-low cost solar cells. Although long-term stability and reliability is a major potential challenge, recent work indicates that 98% stability for months can be achieved via modest changes in the chemistry [6, 7] or fabrication process (e.g., with hot casting) [8]. There have been many studies attempting to significantly improve the stability of perovskite materials. In one recent study, it has been shown that slow photocurrent degradation in thin-film photovoltaic devices is caused by light-activated meta-stable deep-level trap state formation. However, the devices can self-heal completely by resting them in the dark for $>$ 1 min; furthermore, the degradation can be completely prevented by operating the devices at 0°C [9]. More recently, using 2D perovskite materials in a multilayer Ruddlesden-Popper phase, separated by organic *n*-butylammonium (BA) spacer cations, can yield a photovoltaic efficiency of 12.52% without hysteresis [10]. As a result, the devices exhibit greatly improved stability in comparison to their 3D counterparts when subjected to light, humidity and heat stress tests. In particular, it was shown that unencapsulated 2D perovskite devices retain over 60% of their efficiency for over 2,250 hours under constant, standard (AM1.5G) illumination, and exhibit greater tolerance to 65% relative humidity than do three-dimensional equivalents, while encapsulated 2D perovskite devices show an extreme robustness with almost no degradation over 2,250 hours [10].

Optics EXPRESS

This approach has potential to be combined with other approaches, such as using a thin buffer layer plus indium tin oxide (ITO) as a moisture barrier, which can greatly slow down degradation mechanisms in perovskite material system [11]. Furthermore, external encapsulations (glass and/or polymers) [12, 13] can also improve material stability significantly.

Recently, perovskite-crystalline silicon tandem cells have been proposed, with theoretical efficiencies exceeding 30% [4,14,15]. However, measured efficiencies for monolithic tandem cells typically fall between 13% and 21.2% [5, 16], below that of the best single junction crystalline silicon cells [4, 16–18]. On the other hand, spectral splitting and 4-terminal perovskite/silicon tandem cells [19, 20] have higher efficiencies, but potentially requiring higher manufacturing cost compared to the monolithic tandem cells.

Reaching these theoretical limits for tandem cells is still challenging for a variety of reasons. First, the materials used for hole transport layer (HTL) are not sufficiently transparent. For example, Spiro-OMeTAD has been used as the HTL in many world-record perovskite solar cells, but it has a strong absorption peak at 400 nm. Second, bottom junctions made of crystalline silicon require top junctions with bandgaps of 1.7-1.8 eV for the highest performance. In other words, 1.55 eV metal-halide perovskites may suffer a slight open-circuit voltage loss, as well as short-circuit current mismatch. Third, conventional front texturing approaches developed for wafer-based silicon cells are no longer valid for solution processing of perovskites. Thus, new concepts for light trapping are needed to maximize absorption in both junctions of such tandem cells.

Fortunately, there are two potential solutions to these challenges in perovskite/c-Si tandem cells. In the first approach, we introduce manufacturable light-trapping structures for higher short-circuit current (Jsc) values. Our combined electro-optic tandem cell model shows that front-coating layer designs improves the tandem short-circuit current by 2.8 mA/cm^2 [21]. Additionally, recent work on pervoskites indicates that even thinner Spiro-OMeTAD hole transport layer can be used without sacrificing charge collection efficiency [5]. A combination of these approaches will achieve an even larger Jsc gain.

Our recent studies indicate that modifying the perovskite/c-Si tandem architecture to admit light from the back dramatically boosts the area-normalized power output [15, 22]. The basic rationale for this approach is two-fold: (1) significant additional power is available from ground reflection R (the Earth's surface typical shows $R \approx 29\%$ [23]); and (2) current matching constraints are relaxed *significantly*. Our recent work has demonstrated that even with no improvements to subcell performance, an ideal 20% perovskite subcell combined with a 24% c-Si subcell would only yield 25% tandem performance in the typical configuration; whereas 33% normalized power output is possible using a bifacial tandem configuration when $R = 30\%$ [15]. Additional gains are also possible by incorporating future, higher-performance perovskites. The theoretical best case yields a normalized power production of 52%, well in excess of an ordinary tandem or even a bifacial c-Si tandem cell [22]. Despite the promise of a low-cost bifacial architecture, most of the theoretical work to date has been limited to an idealized 1D absorption [15] calculating using a transfer matrix method [24]. Although some full-wave 3D optical simulations have been performed for perovskite solar cells, they have been limited to unifacial architectures with $MAPbI_3$ materials that degrade quickly [25–27].

In this work, to design 2D perovskite/silicon bifacial tandem cells, we first model the optical dispersion of crucial perovskite materials (e.g., $MAPbI_3$, $(BA)_2(MA)_3(Sn_xPb_{1-x})_4I_{13}$, Spiro-OMeTAD, PCBM, PEDOT, TiO_2, etc.) in a particular form that is suitable for the time domain analysis. These dispersion models are then incorporated into finite difference time domain (FDTD) simulations to characterize the quantum efficiency of the 21% world-record perovskite/silicon tandem cells recently reported in the literature [5]. Finally, we design multilayer 2D perovskite based tandem cells using tin-rich perovskites with BA spacers.

Optics EXPRESS

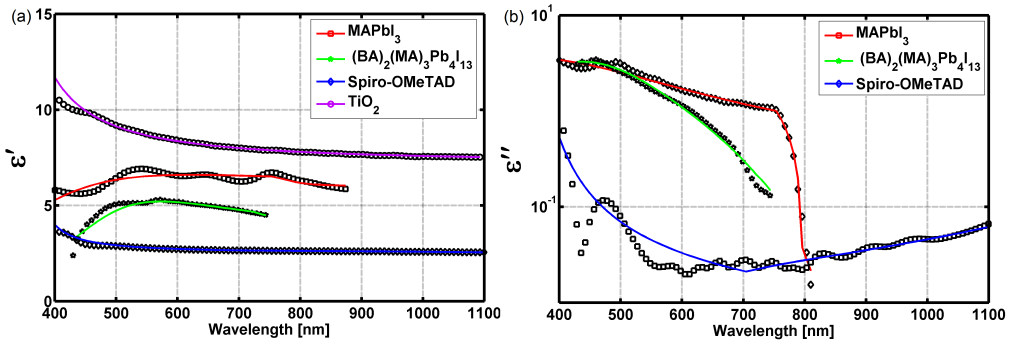

Fig. 1. Photovoltaic material dispersion for both the (a) real and (b) imaginary parts of the relative permittivity. Symbols denote experimental data [10, 28–30], while solid lines are fits to the QCRF model, suitable for FDTD simulation. A close fit is obtained for nearly all data sets, with the exception of the imaginary part of Spiro-OMeTAD. The imaginary part of TiO_2 dispersion is dropped due to negligible absorption in thin film.

2. Methods

2.1. Material modeling

FDTD is a very accurate optical simulation method that directly solves Maxwell's equation over time and space; however, it requires dispersion functions suitable for solution in the time domain [31]. Most semiconductors including photovoltaic materials do not simply follow the Drude-Lorentz model which is the most commonly used dispersion model in FDTD, because of the many optical transitions that are possible above the bandgap energy [32]. In this work, we follow our previously developed dispersion model, called the Quadratic Complex Rational Function (QCRF) [33], to simulate perovskite materials. The QCRF method is more accurate and computationally efficient than conventional dispersion models (e.g., Debye and Drude-Lorentz). Also, it can guarantee a relatively large grid spacing in the FDTD simulation when the material dispersion fitting is numerically validated against von Neumann analysis [34, 35]. The measured complex refractive indices are collected from the literature [10, 28–30]. The refractive indices of tin-rich 2D perovskites ($(BA)_2(MA)_3(Sn_xPb_{1-x})_4I_{13}$) are generated from the refractive index of $(BA)_2(MA)_3Pb_4I_{13}$ [10] plus a uniform, bandgap difference-dependent shift measured in experiment.

As shown in Fig. 1, the modeled time domain dispersion curves match well with prior experiments [10, 28–30]. The imaginary part of the relative permittivity ϵ for $(BA)_2(MA)_3Pb_4I_{13}$ behaves like an indirect bandgap material. Therefore, thin 2D perovskites suffer both incomplete absorption near their bandgap, plus parasitic absorption below their bandgap. Also, the refractive index difference between Spiro-OMeTAD and $MAPbI_3$ is not negligible, which induces Fresnel reflection losses at the materials boundaries, specially when the surface is not textured. Note that we model 2D perovskites ($(BA)_2(MA)_3(Sn_xPb_{1-x})_4I_{13}$), 3D perovskites ($MAPbI_3$, $MASn_xPb_{1-x}I_3$), and charge transport materials (Spiro-OMeTAD, PCBM, PEDOT and TiO_2), but only selected material fittings are shown here for clarity and brevity. The refractive indices of the Sn-rich alloys with BA spacers are assumed with a uniform bandgap shift in the 2D perovskite dispersion data [10], a procedure which has previously been used effectively in other contexts [34]. While prior work alloying Pb-based 3D perovskites with Sn did not yield high stability, it is expected that an encapsulated 2D Pb/Sn perovskite alloy may have superior stability properties, as seen in the 2D Pb perovskite experiment [10].

To further validate our QCRF modeling results, we apply them to FDTD simulations of 300 nm-thick dielectric slabs, and compare to analytical absorption spectra [36, 37]. To calculate analytic

Optics EXPRESS

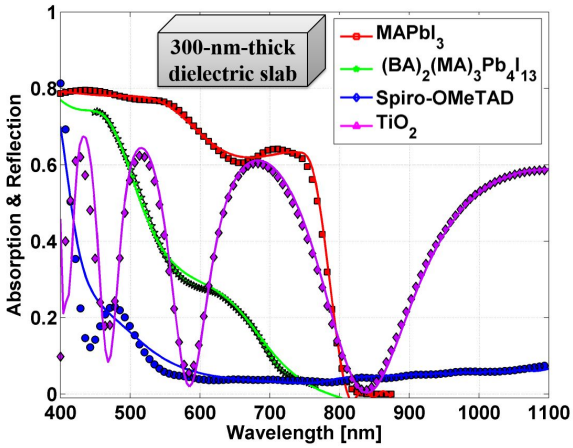

Fig. 2. For each of the modeled photovoltaic materials in Fig. 1, a 300 nm-thick dielectric slab is created; then, the analytical (symbol) and FDTD-simulated (line) absorption (2D, 3D perovskites and Spiro-OMeTAD) and reflection (TiO_2 only) spectra are given above. A close fit is found for all materials across a broad bandwidth, with the exception of Spiro-OMeTAD at short wavelengths.

absorption spectrum, we collected the experimental refractive index data from the literatures [10, 28–30] and then compute absorption of 300-nm-thick dielectric slab via multiple reflections and transmissions [36]. Figure 2 shows very good agreement between theory and simulation overall, with the exception of Spiro-OMeTAD at short wavelengths. $(BA)_2(MA)_3Pb_4I_{13}$ may require substantial light trapping for thin films, due to significant incomplete absorption, as observed in experiment [10].

2.2. Tandem perovskite/silicon cell modeling

The co-exitence of multiple loss components in a tandem cell make it difficult to isolate the light harvesting efficiency (and thereby the material quality) of the absorbers. Especially for light scattering and trapping solar cells, quantifying the fractional absorption of each loss component is much harder. Here, we use both 3D FDTD simulations and experiments to analyze the quantum efficiency of light trapping tandem cells [5]. In this work, photo-current and parasitic absorption are all quantified in units of mA/cm^2, which can be calculated by:

$$J_{ph} = \int_{300\ nm}^{1100\ nm} d\lambda \left[\frac{e\lambda}{hc} \frac{dI}{d\lambda} A(\lambda) \right], \tag{1}$$

where $A(\lambda)$ is a simulated fractional absorption for each photovoltaic layer, and $\frac{dI}{d\lambda}$ indicates the light intensity reaching the solar cell per unit wavelength (given by the AM1.5G solar spectrum).

For a light trapping tandem cell shown in Fig. 3(a), a simulated total absorption spectrum is compared to the same quantity measured in experiment [5]. Note that the absorption of the wafer-based silicon layer is approximated by a physics-based extrapolation [21]. As shown in Fig. 3(a), the experimental (black dashed line) and simulated total absorption (red dashed line) agree very well, with a root-mean-squared percent error of 2.26%, which increases our confidence in the following loss calculation (filled plot) in the same figure. The total absorption A in the simulation is computed as $A = 1 - R$ (where R is the reflected flux), while the fractional absorption of each loss component is calculated by the net transmitted electromagnetic flux at the material boundary. Now, we define Absorber Light Harvesting Efficiency (ALHE), which can be calculated as the experimentally measured EQE divided by the simulated perovskite (or

Optics EXPRESS

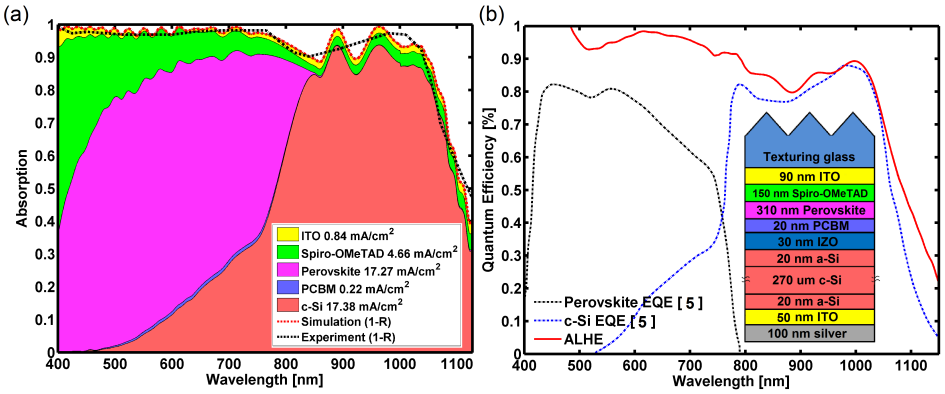

Fig. 3. (a) Optical loss analysis of the world-record experimental perovskite/silicon tandem cells [5]. Reflection and Spiro-OMeTAD parasitic absorption are the major loss components over wavelengths ranging from 400–1127 nm. Ideal quantum efficiency is assumed for quantifying photo-current. The dashed lines indicate total absorption (= 1 − R) for both experiment [5] and simulation. (b) The calculated Absorber Light Harvesting Efficiency (ALHE) shows that the perovskite layer does not suffer much electrical losses, while the c-Si layer has recombination losses. The inset figure indicates a simulated perovskite/silicon tandem structure. Note that ALHE slightly exceeds 100 % at the shorter wavelengths due to a modeling error of Spiro-OMeTAD shown in Fig. 1(a).

c-Si) layer absorption. The calculated ALHE in Fig. 3(c) shows that the perovskite layer does not suffer much electrical loss, while the c-Si layer has recombination losses at longer wavelengths. This analysis suggests that electrical losses in the crystalline silicon bottom junction must be reduced. The two major barriers to ideal optical performance are Spiro-OMeTAD parasitic losses and reflection losses in this tandem cell. Unfortunately, light trapping on the front-side may also increase Spiro-OMeTAD losses, canceling out the potential benefit. Also, a conformal texturing technology, which can potentially increase light trapping further, may not be compatible with perovskite/silicon tandem cells due to manufacturing constraints [5]. Alternatively, a plasmonic back reflector or dielectric back grating can be used to improve light trapping of this tandem cell without inducing optical parasitic losses [38, 39]. In summary, the world record monolithic perovskite/silicon tandem cell has already reached near unity (i.e., ideal) ALHE, while it still suffers a significant amount of parasitic losses and reflection loss. This indicates that the initial performance of the perovskite layer itself need not be improved, but the surrounding layers can still benefit from further research.

3. 2D perovskite/silicon bifacial tandem cell design

Recently, 2D perovskites have been shown to offer extraordinary *intrinsic* material stability compared to corresponding 3D perovskites [10]. Furthermore, they offer flexible bandgaps, depending on their precise material composition. Therefore, 2D perovskites are promising as the top cell materials for long-term stable high efficiency tandem cells. However, Jsc values obtained by single junction 2D perovskite have so far been limited to 16.76 mA/cm^2 due to incomplete light absorption [10]. Thus, a new light trapping strategy is needed to improve its efficiency further. The other meaningful progress for developing a top junction material of tandem cells has been made in tin-rich low-bandgap perovskite solar cells [40]. Tin-rich perovskite solar cells show an adjustable bandgap with relatively high open circuit voltage which is very important for tandem solar cells. Here, we combine tin-rich perovskite and BA spacer cations together to make high-stability tunable-bandgap top junction materials. Depending on the tin ratio in

Optics EXPRESS

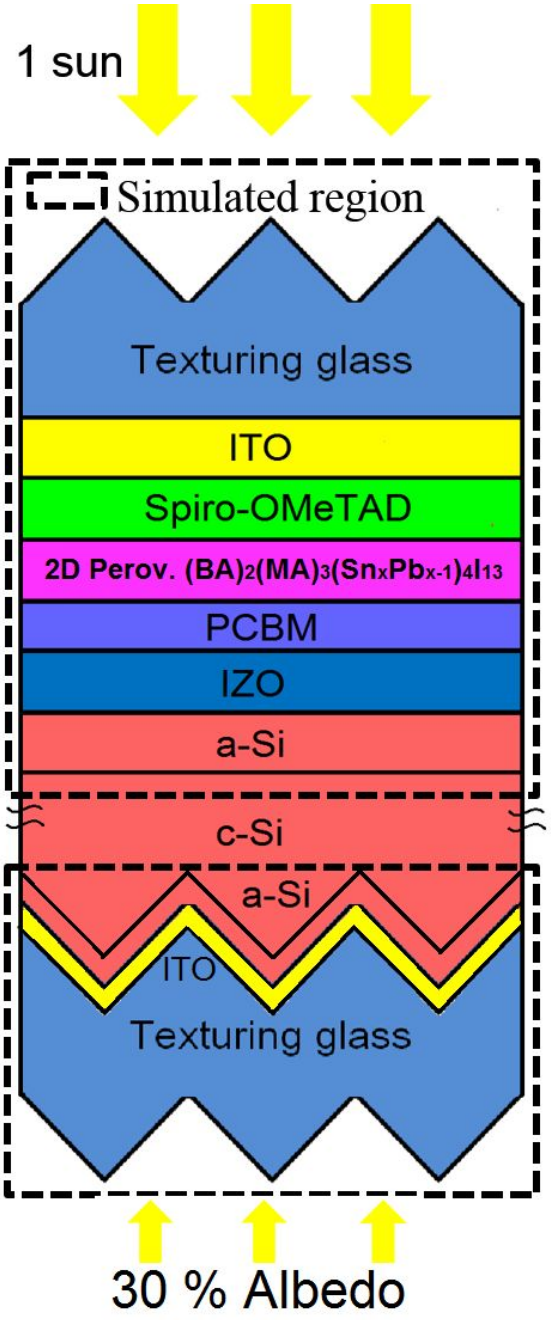

Fig. 4. 3D FDTD simulation geometry. The front and rear sides have pyramidal texturing with 1 μm periodicity and 54.7 degree opening angle. Material thicknesses for glass/ITO/Spiro-OMeTAD/2D perovskite/PCBM/IZO/a-Si/c-Si/a-Si/ITO are 2μm/90 nm/160 nm/200 nm–450 nm/20 nm/30 nm/20 nm/270 μm/20 nm/70 nm, respectively. The dashed line indicates an actually simulated region. The fractional absorption of a c-Si wafer is computed by a physics-based approximation [21].

Optics EXPRESS

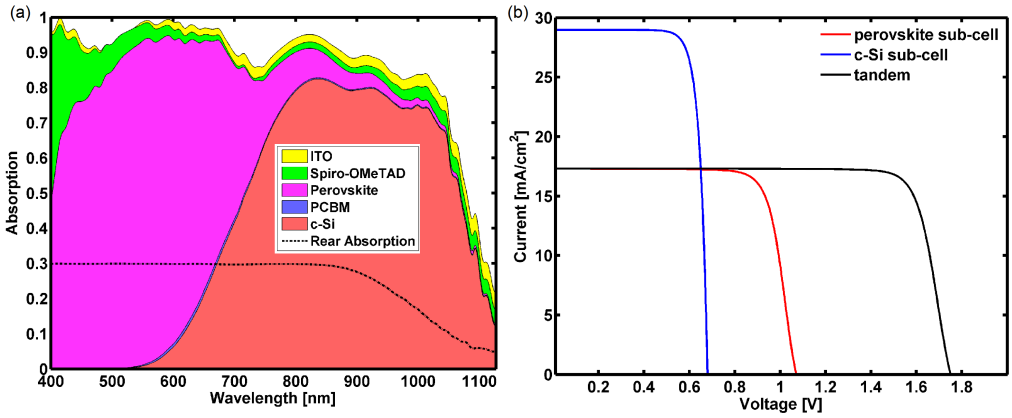

Fig. 5. (a) Optical loss analysis for $(BA)_2(MA)_3Pb_4I_{13}$/silicon bifacial tandem cells. The integrated Jph for 2D perovskite, c-Si(from front) and c-Si(from rear) are 17.32 mA/cm^2, 18.38 mA/cm^2, 11.65 mA/cm^2, respectively. Normalized power output for this bifacial tandem is 23.13%. (b) I-V characteristics, as calculated by a combination of the optical loss analysis in (a), plus a validated physics-based compact model [41].

$(BA)_2(MA)_3(Sn_xPb_{1-x})_4I_{13}$ materials, bandgaps as low as 1.1 eV can be achieved [40]. Paired with a bottom silicon junction, the ideal bandgap for a top junction is around 1.7 eV for a monofacial architecture, or 1.55 eV for a bifacial architecture with 30% albedo [22].

However, these ideal top junction bandgaps may not be always true when non-ideality factors play a role. For example, parasitic absorption of longer wavelengths may red-shift the ideal bandgap. This issue is particularly relevant in perovskite solar cells containing parasitically absorbing materials like Spiro-OMeTAD. Incomplete absorption, which is observed in perovskite/silicon tandem cells [5], may also affect the ideal material selection of the top junction. In this section, we take all these non-idealities into account to design optimized 2D perovskite/silicon bifacial tandem cells for high normalized powers and long-term stability.

In this work, 30% albedo is assumed, which is the average reflectance value of Earth [23]. It could also be much higher, if the ground material of a solar farm is chosen appropriately [42]. Figure 4 shows our 3D simulation geometry. A pyramidal texturing with a 54.7° opening angle is applied to the front/rear glasses, while other layers have a planar surface which may not cause extra carrier collection losses in real experiments. However, the rear side silicon surface is conformally textured, which is commonly used in the HIT solar cell architecture [43, 44]. Note that silicon wafer absorption is approximated with a physics-based model [21], using transmitted flux at the silicon material boundary. Rear side illumination with 30% albedo is simulated only once, resulting in an extra 11.65 mA/cm^2 of photo-current in the bottom junction only.

As shown in Fig. 5(a), $(BA)_2(MA)_3Pb_4I_{13}$ is simulated here. Due to the assumption of a flat material boundary, it suffers a relatively large amount of Fresnel's reflection. This could be addressed by optimizing refractive index and thickness of the charge transport materials [45]. However, in this work, to design an experimentally feasible architecture, we assume that their refractive indices and thicknesses are not tunable and perovskite material boundaries are not able to be textured. Figure 5(b) shows a current-voltage characteristic, calculated using a physics-based compact model [41,46]. The perovskite compact model describes the operation of different kinds of perovskite solar cells by accounting carrier selective transport layers and voltage-dependent carrier collection. The integrated Jph calculated in (a) provides the maximum absorption (Gmax) utilized in the compact model. Furthermore, we assume that adding BA spacers to 3D perovskites only affect the optical but not electrical properties, which is reasonable for sufficiently thin layers.

Optics EXPRESS

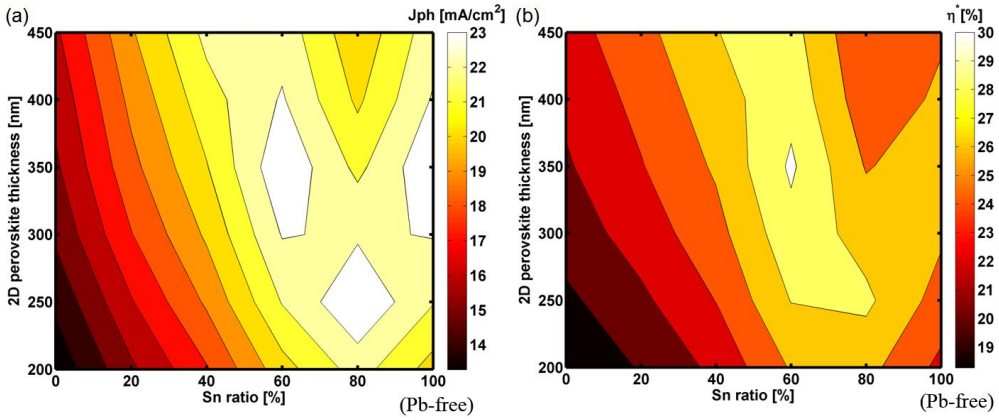

Fig. 6. (a) Jph versus both 2-D perovskite thickness and Sn ratio. The three Jph peaks are found at 60 % Sn ratio with a 350-nm-thick perovskite(23.83mA/cm^2), 80 % Sn ratio with a 250-nm-thick perovskite(23.90mA/cm^2), 100 % Sn ratio with a 350-nm-thick perovskite(23.83mA/cm^2). (b) Efficiency versus both 2-D perovskite thickness and Sn ratio. The detailed method for calculating normalized power output is discussed in the main text.

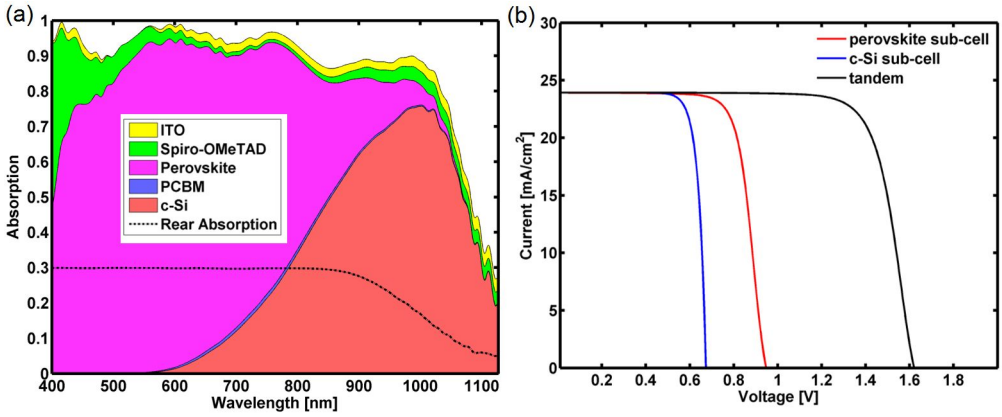

Fig. 7. (a) Optical loss analysis for $(BA)_2(MA)_3(Sn_{0.6}Pb_{0.4})_4I_{13}$/silicon bifacial tandem cells. The integrated Jph for 2D perovskite, c-Si (from front) and c-Si (from rear) are 23.95 mA/cm^2, 12.28 mA/cm^2, and 11.65 mA/cm^2, respectively. Normalized power output for this bifacial tandem is 30.31%. (b) I-V characteristics, as calculated by a combination of the optical loss analysis in (a), plus a validated physics-based compact model [41].

Our simulation results indicate that pure Pb-based 2D perovskite/silicon tandem cells have fairly well-matched Jph values in a monofacial architecture; however, in a bifacial scheme it suffers significant current mismatch. Thus, it might be more applicable to the conventional monofacial architecture due to its relatively high bandgap (1.6 eV) [10].

Now, we vary both Sn ratio and perovskite thickness of $(BA)_2(MA)_3(Sn_xPb_{1-x})_4I_{13}$ to search for an optimum design of this class of tandem cells. Figure 6(a) shows three local optima in white. The first Jph optima is found at a 60% Sn ratio with a 350-nm-thick perovskite (23.83 mA/cm^2) and the second Jph optima is found at an 80% Sn ratio with a 250 nm-thick perovskite (23.90 mA/cm^2) and the last optima is found at a 100% Sn ratio (i.e., Pb-free) with a 350 nm-thick perovskite (23.83 mA/cm^2). If we assume that they all offer the same charge collection efficiency, then $(BA)_2(MA)_3(Sn_{0.6}Pb_{0.4})_4I_{13}$ will have the highest efficiency due to

Optics EXPRESS

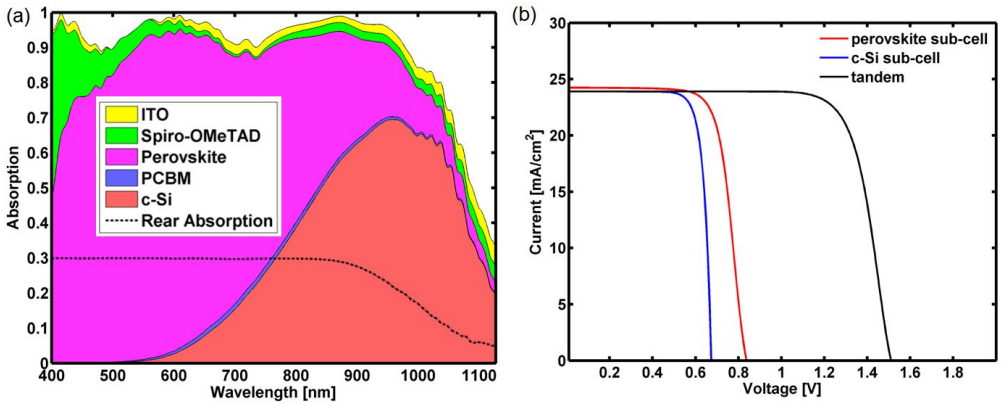

Fig. 8. (a) Optical loss analysis for $(BA)_2(MA)_3(Sn_{0.8}Pb_{0.2})_4I_{13}$ /silicon bifacial tandem cells. The integrated Jph for 2D perovskite, c-Si(from front) and c-Si(from rear) are 24.28 mA/cm^2, 12.25 mA/cm^2, and 11.65 mA/cm^2, respectively. The normalized power output for this bifacial tandem is 28.41%. (b) I-V characteristics calculated by combining the optical loss analysis in (a) and a validated physics-based compact model [41].

the highest Voc [40]. As shown in Fig. 6(b), the normalized power output of the bifacial tandem cell is calculated with assuming 76% fill factor measured in the experiment [40] and measured Voc for a c-Si subcell Voc [43] and 2D perovskite subcell [40] with a 0.156 V blue-shift, caused by the 2D perovskite spacers. In this calculation, the peak normalized power production of 30.31% is found at a 60% Sn ratio with a 350-nm-thick perovskite. This calculated efficiency could increase more with further enhancements of 2D perovskite material quality [10].

Figure 7(a) shows the optical loss analysis for the optimum $(BA)_2(MA)_3(Sn_{0.6}Pb_{0.4})_4I_{13}$/silicon bifacial tandem cells. The matched Jph is 23.93 mA/cm^2 in this bifacial tandem cell with assuming 30 % albedo. Both the Spiro-OMeTAD parasitic absorption (2.28 mA/cm^2) and the Fresnel's reflection loss (2.77 mA/cm^2) are major optical loss mechanisms here. Thus, Jph can be improved further by a transparent hole collecting material and optical path length optimization [45]. In particular, preliminary modeling results show that replacing the hole transport layer with a thinner one and/or reversing the stacking order could be beneficial, but further experimental advances would be needed to realize such a strategy. The corresponding I-V curve for the optimum design is shown in Fig. 7(b) using physics-based compact models for both subcells [41, 46].

Finally, the optical loss analysis for the local Jph optima at 80% Sn with a 250 nm 2D perovskite thickness is plotted in Fig. 8. Because the optimum perovskite thickness (250 nm) for $(BA)_2(MA)_3(Sn_{0.8}Pb_{0.2})_4I_{13}$ is much thinner than other material compositions, this local optima may have great potential as a specific target for future experiments. As discussed in the experimental paper [10], 2D perovskites could be more sensitive to material thickness due to their limited electronic mobilities. Detailed optical losses for different tin ratios are shown in Table 1.

These findings demonstrate how experimentally realizable 2D perovskite/silicon bifacial tandem cells can be designed while accounting for previously observed non-idealities [5, 10, 40]. The particular combinations of 80% Sn 2D perovskites with a 250 nm thickness and 60% Sn 2D perovskites with a 350 nm thickness seem most relevant for experiments, with normalized power production up to 30.31%. Also, any future improvements in material quality, light trapping (including textured perovskite syntheses) and improved transparent charge transport layer materials could further increase the predicted bifacial power output.

Optics EXPRESS

Table 1. Optical losses in terms of Jph [mA/cm^2]

Sn [%]	Perov. thick.	Refl.	ITO	Spiro-OMeTAD	Perov.	c-Si (front)	c-Si (rear)
0	450 nm	3.36	1.12	2.29	17.32	18.38	11.65
60	350 nm	2.77	1.02	2.28	23.95	12.28	11.65
80	250 nm	2.14	1.07	2.28	24.28	12.25	11.65

4. Conclusion

In this work, to achieve high-efficiency, low-cost and long-term stable solar cells, we investigated bifacial tandem cells using 2D perovskite materials on top of a crystalline silicon solar cell. To build an accurate simulation framework, we first model perovskite materials in the time domain and validate them against theory and experiment. Using the model, we quantified both optical and electrical losses separately for perovskite/silicon tandem cells by comparison with measured EQE, and then simulated the fractional absorption of each layer. This novel characterization method reveals the hidden loss mechanisms for light trapping perovskite/silicon tandem cells. Then, we design Sn-based 2D perovskite/silicon bifacial tandem cells which are intrinsically much more stable than their 3D perovskite counterparts. The optimum designs use 60% Sn 2D perovskites, which have a maximum photo current of 23.95 mA/cm^2 with 30% albedo, corresponding to 30.31% normalized power output. This efficiency calculation is obtained with reference to existing subcell performances. In addition, it is shown that Pb-free 2D perovskite/silicon bifacial tandem cells can achieve over 27% normalized power production.

Acknowledgments

The authors thank Raghu Chavali, Reza Asadpour, and Aditya Sadhanala for valuable discussions. Support was provided by the Department of Energy, under DOE Cooperative Agreement No. DE-EE0004946 (PVMI Bay Area PV Consortium), through the NCN-NEEDS program, which is funded by the National Science Foundation, contract 1227020-EEC, through the CAREER award program, which is funded by the National Science Foundation under Award No. 1454315-EEC, which is also funded by the LDRD program and LANL, and finally by the Semiconductor Research Corporation.